Chapter 6

Adsorption using AC

6.1 Removal of Cu^{2+}, Ni^{2+} and Zn^{2+} ions by Activated Carbon derived from *Tectona grandis*

The USEPA has designated activated carbon as a superior adsorbent in the adsorption process as one of the most successful environmental pollution management technologies ever reported [387]. Cost-effectiveness of activated carbon is another key factor to take into consideration. Recently, activated carbon generated from agricultural waste has mostly been synthesised as a more cost-effective alternative to commercially available activated carbon. [388]–[390]. The raw material selection for activated carbon synthesis is determined by properties such as low inorganic compound concentrations for high carbon, lower ash content and volatile material content, minimal cost, low storage degradation rate, activation potential, and higher yield [391], [392].

In the sawmill sector, waste sawdust accounts for 15% to 20% of overall production [173], [174]. That is a big number and it is not being used to its full potential. 47.5% cellulose and 29.9% lignin are the most important components of *Tectona grandis* wood. The existence of cellulose suggests that it can be used as an adsorbent [173]. Sawdust from the *Tectona grandis* tree is cost - effective, unused, and a byproduct. [175]. The high carbon concentration of *Tectona grandis* sawdust (about 50%) is a notable feature of a putative

activated carbon precursor [176].

In light of these facts, the present study tried to generate activated carbon (AC) that was synthesised from *Tectona grandis* sawdust using $Na_2S_2O_3$ as an oxidising agent using a green technique. In the context of this study, green synthesis/ routes means that we have used sustainable and cost-effective carbon precursors with safe activating chemical agents to produce AC, which reduced the production of hazardous sub-products and secondary chemical sludge. In this study, the *Tectona grandis* sawdust was used to create very porous carbon using this synthesis process.

The present study aimed at the use of AC for removal of Cu^{2+}, Ni^{2+} and Zn^{2+} ions from wastewater. In addition to this, physico-chemical characterization of AC, optimization study, adsorption dynamics, isotherm, kinetic, mechanistic and thermodynamic correlations were studied in detail in order to understand the basic mechanism of metal ions on the AC surface. ANN tool of MATLAB has been used to compare the experimental result with the predicted outcome. Finally, a comparative analysis of AC with other adsorbents reported by other researchers has been also presented.

6.2 Results and Discussion

6.2.1 Characterization

6.2.1.1 SEM-EDX

The SEM of AC has been depicted in Figure 6.1. Figure 6.1a shows that the AC surface has protrusions that run through the biomass matrix [391]. Diasporic particle size distribution revealed a wide range of forms and sizes for the activated carbon particles.An additional feature of the activated carbon particles was their rough and layered surface, which had the resemblance of a loose sponge. [393]. The activating agent, in this case $Na_2S_2O_3$, causes surface discontinuity in AC, as seen in SEM (Figure 6.1).

After adsorption of Cu^{2+}, Ni^{2+} and Zn^{2+} ions, there is clear difference in the surface morphology of AC and shown in Figure 6.1b. The surface heterogeneity in AC helps in ad-

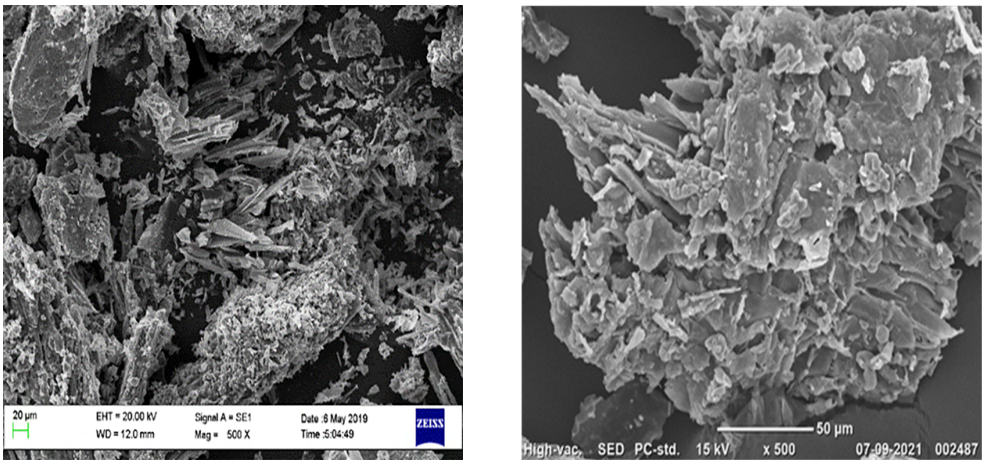

(a) Before adsorption **(b)** After adsorption

Figure 6.1: SEM of AC

sorption of metal ions. Carbonization-induced dehydration was principally responsible for the well-developed porosity and subsequent increase in surface area, which reached 1270 m^2/g [330]. Bardalai et al., 2019 [394] detected flaky bits at a magnification of 500 X. Nguyen et al., 2019 [395] discovered that the surface of activated carbon was not uniform by inspecting SEM micrographs. All of these features were found to be identical to those of the activated carbon created in this research.

The EDX of AC is depicted in Figure 6.2 and Table 6.1.

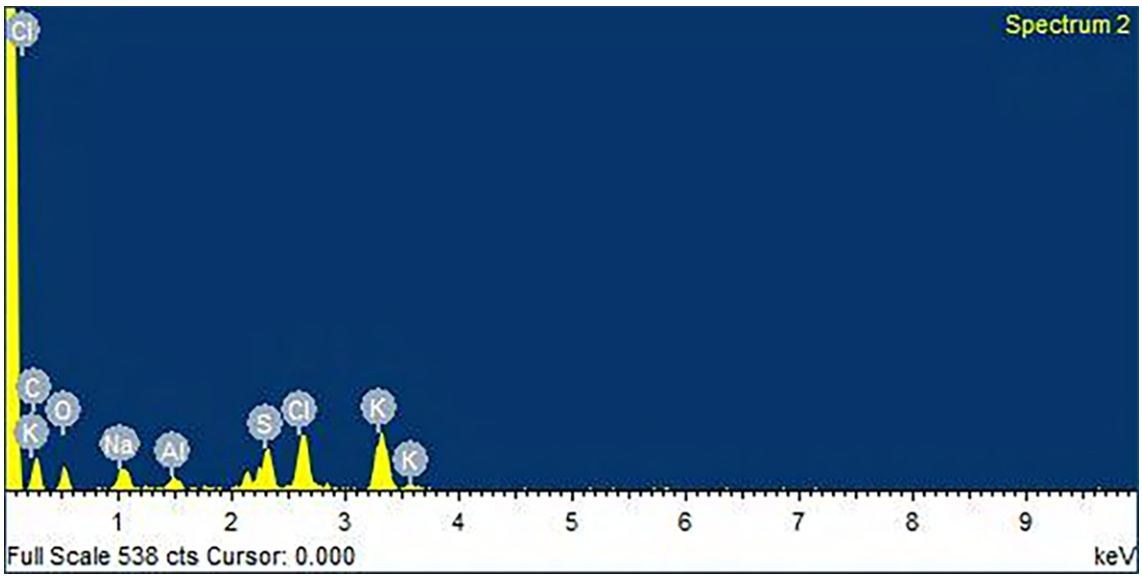

Figure 6.2: EDX of AC

According to the EDX data, the macropore crystals contained sulphur, sodium, potassium, and chlorine compounds (Figure 6.2). The presence of several compounds in the AC was

Table 6.1: Percentage of elemental weight from AC's EDX

Element	Weight (%)
C K	43.56
O K	26.41
Na K	3.65
Al K	1.46
S K	4.86
Cl K	8.95
K K	11.11
Total	**100.00**

shown by the EDX. The activation of TG in the presence of $Na_2S_2O_3$ and KCl caused this. Mopoung et al., 2015 [396] investigated the properties of activated carbon made from tamarind seeds using potassium hydroxide activation and EDX revealed a significant potassium content due to the potassium hydroxide activation. EDX in Figure 6.2 also depicts the presence of several elements on the surface of AC in various atomic and weight percentages. The existence of potassium chloride accounts for the presence of K and Cl, whereas sodium thiosulphate accounts for the presence of Na and S. These findings were comparable to those of Mopoung et al., 2015 [396]. As a result of these findings, activating reagent is present on the surface of AC, which is compatible with the SEM result, which indicates that there are crystals of reagent ($Na_2S_2O_3$) on the surface of AC..

6.2.1.2 FTIR

FTIR analysis was utilized to assess the surface chemistry of TG and AC. 6.3 depicts the FTIR spectra of AC and TG.

The FTIR spectra of TG and AC revealed the presence of alcohols and phenols in the structure via the O-H stretching vibration about 3400 cm^{-1}. TG has an absorption band near 2900 cm^{-1}, indicating the existence of aromatic ring stretching (phenolic groups). In both TG and AC, the C=O stretching vibrations at 1734, 1653, and 1633 cm^{-1} indicated the presence of carbonyl group in ketones, phenols, carboxyl acids, and aldehydes [388],

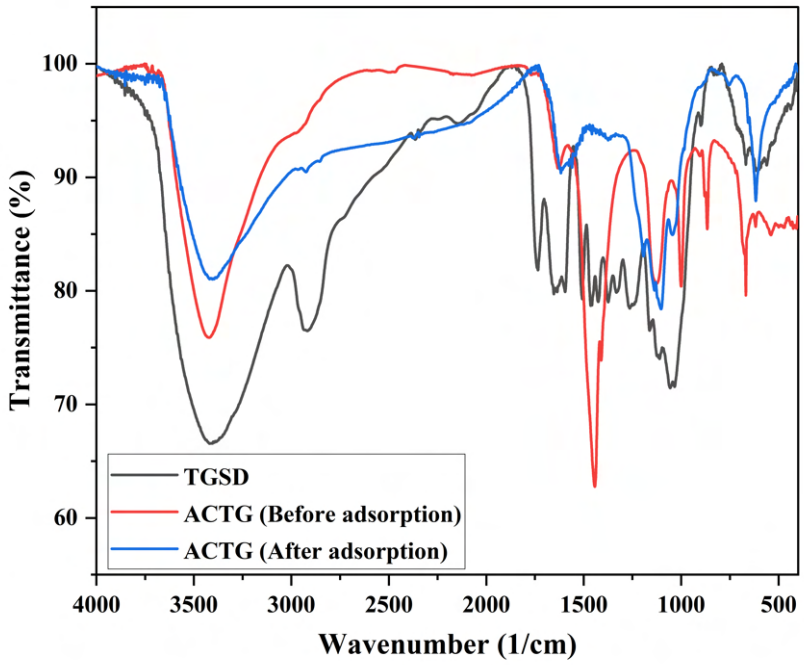

Figure 6.3: FTIR of TG and AC (before and after adsorption of ternary metal ions)

[389], [392]. Near 1400 cm^{-1}, the absorption peak was attributed to the S=O group of TG and AC. This peak (1400 cm^{-1}) was observed to be stronger in AC. Both TG and AC exhibited bands near 1000 cm^{-1} that exhibit C-H and C-OH stretching vibrations. This is owing to the presence of multiple functional groups on the surface of TG and AC [397]. Additionally, aryl halide (C_6H_5-X or Ar-X where X = F, Cl, Br, and I) and alkenes (C=C) were found on the surface of TG and AC, with absorption peaks at 866 and 668 cm^{-1}, respectively [398]. The missing, shifting, or presence of bonds indicated that AC exhibited chemical change post activation. Surface pore formation was exacerbated as a result of the removal of many functional groups in AC [399], [400]. After adsorption, some peaks disappear due to adsorption of Cu^{2+}, Ni^{2+} and Zn^{2+} ions on the surface of AC and the changes are listed in Table 6.2 and shown in Figure 6.3. FTIR peaks recorded before and after the activation method of sawdust, as well as before and after the adsorption of AC are shown in Table 6.2 in the form of a comparative table.

Biochar generated from teak sawdust was evaluated by Bardalai et al., 2019 [394], who identified a peak at 3411 cm^{-1}, indicating the presence of the -OH group resulting from dehydration of the cellulose and hemicellulose present in teak sawdust. Lignin aromatic vibrations are also responsible for bands between 1600 and 1511 cm^{-1}. These bands were

also found in present study, indicating that they belong to the same functional categories.

Table 6.2: Table of FTIR comparisons before and after activation of sawdust

Wavenumber (1/cm) forTG	Wavenumber (1/cm) for AC (Before adsorption)	Wavenumber (1/cm) for AC (After adsorption)	Bond	Functional group
3419.55	3422.27	3409.84	O-H stretching	Alcohol and phenol
2916.81	-	-	$-C_6H_5$	Phenolic group
1734.73	-	-	-CO-	Ketone
1653.33	1633.63	1618.87	-C=O	Carboxyl acid
1465.38	1443.20	-	S=O stretching	Sulfate
1056.48	1000.24	1109.98	C-N stretching	Amine
826.81	866.26	-	C-Cl stretch	Aryl halide
670.86	668.29	614.22	C=C bending	Alkene

6.2.1.3 XRD

The crystallinity of AC was determined using X-ray diffraction analysis. The pattern was examined at angles ranging from 10 to 80º (2θ).The degree of crystallinity was determined by comparing the regions under crystalline peaks to the regions under the amorphous curves [401].

The crystallinity and amorphousness of the AC were found to be 13.48%and 86.52% in this study. In the XRD pattern (Figure 6.4), two diffractive peaks at 24.08º and 44.24º were seen, indicating the amorphous behavior of graphitic carbon (002) and (101), respectively [185], [402]. The presence of cellulose in the AC was shown by a band near 24º [403].

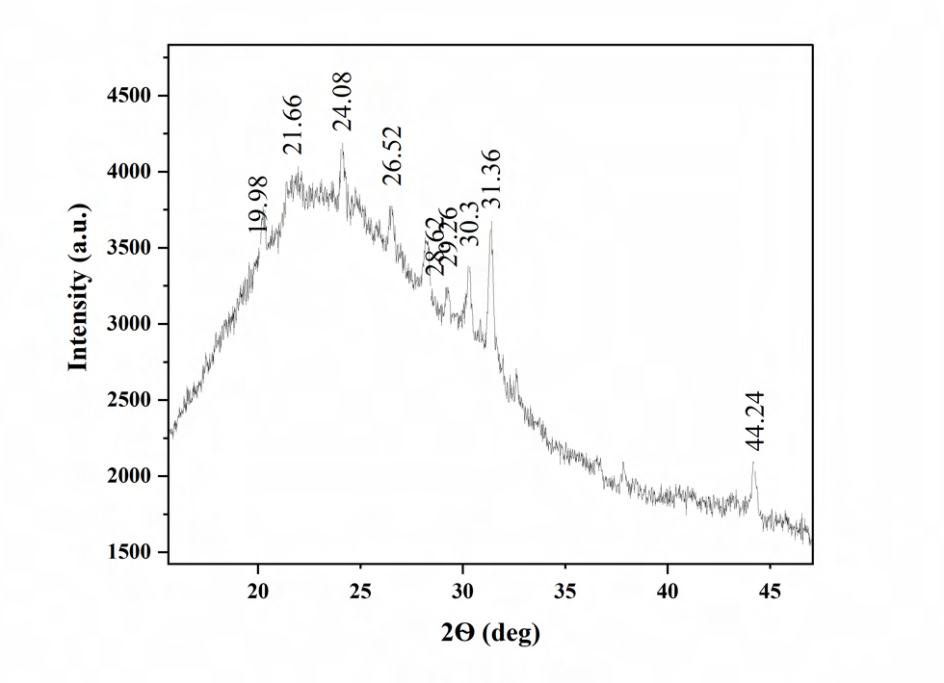

Figure 6.4: XRD analysis of AC

Shamsuddin et al., 2015 [404] demonstrated the same XRD pattern. The graphite-like structure normally forms on activated carbon; however Bardalai et al., 2019 [394] observed the same structure in biochar with maxima of 3.35 Å and 2.03 Å that corresponded to 26.6° and 44.5°, respectively. Similar peaks were observed in this investigation at interplane spacings (d) of 3.4 Å and 2 Å, which equate to 26.52° and 44.24°, respectively (Table 6.3). Thus, the presence of graphite-like structure on AC was concluded. Calcite ($CaCO_3$) has been identified in AC with peaks at 3.1 Å (d), which correlate to two temperatures of 28.62° and 29.26°. Microbiologically precipitated calcite has a wide range of applications, including soil recovery, soil stabilization, and concrete restoration. Peaks at 24.08° with 3.7 Å (d) revealed the existence of whewellite in AC [394].

Bardalai et al., 2019 [394] reported an amorphous activity in biochar generated from teak tree sawdust in an XRD analysis of the material. Through comparison with other researchers' findings, it was possible to establish and confirm the presence of amorphous behaviour in AC in the present study. The XRD analysis of AC is shown in detail in Table 6.3.

Table 6.3 revealed that small crystallite sizes resulted in broad peaks (full width at half maximum (FWHM)) [195].

Table 6.3: XRD analysis of AC

Sl no.	Area	Area Intg P (%)	Row Index	Beginning X	Ending X	FWHM	2θ (°)	d (Å)	Height
1	17045.2	20.57	750	19.95	19.995	5.01	19.98	4.4	2765
2	8538.69	10.30	834	20.1	22.94	2.82	21.66	4.1	3295
3	9738.19	11.75	955	22.94	26.16	3.2	24.08	3.7	3448
4	6071.58	7.32	1077	26.16	28.42	2.24	26.52	3.4	3092
5	768.6	0.92	1182	28.42	28.74	0.3	28.62	3.1	2497
6	2713.45	3.27	1214	28.74	29.9	1.14	29.26	3.1	2556
7	1624.13	1.96	1266	29.9	30.58	0.66	30.3	2.9	2691
8	18133.6	21.88	1319	30.58	43.62	3.49	31.36	2.9	2938
9	18093.7	21.84	1963	43.62	79.44	7.12	44.24	2	1348

6.2.1.4 TGA

Figure 6.5 showed that at temperatures below 150°C, there was a loss of water in AC.

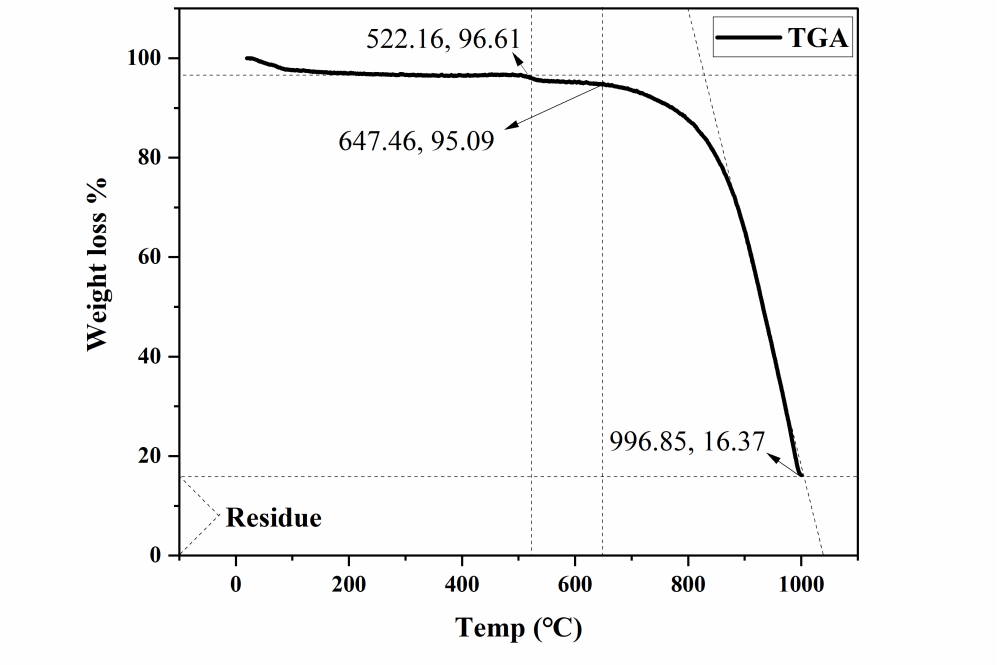

Figure 6.5: TGA of AC

The breakdown of low molecular weight molecules occurred when the temperature was raised to 250°C. Thermo-oxidative breakdown of AC was then detected as the temperature

was increased from 250 to 500°C. Above 500°C, hydro carbonated substances began to carbonize [405]. There was no weight loss in AC when the temperature was raised from 500°C to 522.16°C. Above 522.16°C, a modest decrease in the mass of AC was observed up to 647.46°C, and beyond 647.46°C, a severe decrease in the weight of AC was detected until the temperature reached 996.85°C. At 996.85°C, the approximate weight loss was roughly 16.37 %. Only until 600°C, there was considerable weight loss, which revealed the destruction of cellulose and lignin in AC [394]. The quick carbonization of the AC resulted in a drop in weight after 647.46°C [392], [406].

6.2.1.5 BET Surface Area

This is one of the significant aspects to consider when evaluating activated carbon's adsorption capacity. It is well known that a larger surface area means more active sites are available, making the material more adsorption-friendly [329], [330]. The BET surface area and total pore volume of AC were calculated to be 1270 m^2/g and 0.673 cm^3/g, respectively in this study.

According to Shrestha et al., 2018 [185] the BET surface area of the produced activated carbon was 10.45 m^2/g. The observed surface area was too small in comparison to other activated carbons. This is due to the breaking down of micro and mesopore walls, as well as the creation of macropores. Ismadji et al., 2005 [407] used vacuum pyrolysis of teak sawdust to produce activated carbon with a BET surface area of 1150 m^2/g. As a result, when compared to other activated carbons, the activated carbon generated in this study performed significantly better in terms of BET surface area.

6.2.1.6 Proximate analysis

Table 6.4 shows proximate analysis of TG. TG's high carbon and low ash concentration suggested that it could be an effective carbon precursor [392]. The higher volatile matter content in TG was due to the presence of organic components [391]. Ekpete et al., 2017 [399] investigated the synthesis and characterization of activated carbon derived from the fruit stem of Plantain (*Musa paradisiaca*). Due to the low quantity of moisture, ash, and

volatile matter, the author noted that particle density was relatively low. The findings of Ekpete et al., 2017 [399] were similar to those of the present study. Shrestha et al., 2018 [185] conducted an in-depth analysis of activated carbon made from sal sawdust and discovered a decreased ash level, indicating that the precursor included little inorganic materials. Kongsomart et al., 2015 [183] used teak sawdust to produce activated carbon. Authors also observed that the precursor material had a low moisture and ash content. Similar results were obtained in the present work.

Table 6.4: Proximate analysis of TG

Ash	Moisture	Volatile matter	Fixed carbon
0.7	18.3	13.7	67.3

6.2.1.7 Yield (%)

The yield of TG for generating AC was 52% (SD ± 0.41%) in the present study. Srinivasakannan et al., 2004 [188] reported an yield of 35 % during the production of activated carbon from rubber wood sawdust. Zhang et al., 2010 [408] demonstrated that the yield of activated carbon production is proportional to the impregnation ratio.

6.2.1.8 Bulk Density

The bulk density of AC was calculated as 0.42 g/cm^3 [409]. The lower bulk density estimates revealed a carbon structure that is extensively branched and porous, with more void space [410]. An appropriate adsorbent has a reduced bulk density value. The presence of micropores in the structure was reported by the bulk density [333]. The apparent bulk density of AC was determined to be lower than the maximum permitted limit given by the ASTM, which is 0.42 - 0.52 g/ cm^3 [334].

6.2.1.9 Iodine Number

The carbon prefers to adsorb small molecules. The amount of iodine adsorbed per unit mass of carbon is one approach to assess AC's adsorption capacity. It's a rough measure-

ment technique for estimating surface area and micropore density, as well as an activity level indication (higher is the number, higher is the activation rate). The ideal iodine number range for adsorbents is typically 500 to 1200 mg/g [396]. The iodine number of AC was 782 mg/g (SD ± 0.27) [411]. Shrestha et al., 2018 [185] examined activated carbon made from sal sawdust in detail and found an iodine number of 534.6, suggesting the presence of micropores in the sample. In the process of turning rubber wood sawdust into activated carbon, Srinivasakannan et al., 2004 [412] recorded an iodine number of 1096. As others researchers have reported and validated in the present study, the presence of micropores in AC was confirmed by the iodine number.

6.2.2 pH_{ZPC}

By constructing a curve between the initial and final pH values of AC, the pH_{zpc} was determined (Figure 6.6).

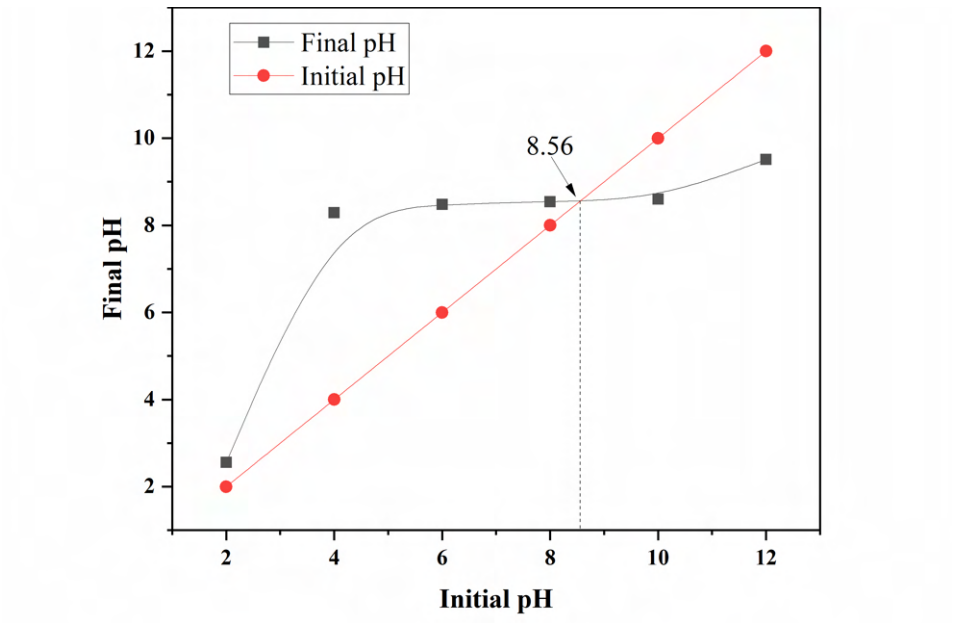

Figure 6.6: pH_{zpc} of AC

The point at which two curves overlap is the sample's zero-point charge pH. The pH_{zpc} value obtained in this study was 8.56. At a value smaller than 8.56, this value indicated that AC was positively charged [398], [413]. Singh et al., 2011 [414] observed that raw sawdust had a pH_{zpc} of 7.29 while treated sawdust had a pH_{zpc} of 6.68. According to their

investigation, a low pH value favored dye adsorption by attracting negatively charged dye ions via electrostatic attraction.

6.2.3 Adsorption Dynamics

In the present work, values of the film and pore diffusivity coefficients showed that adsorption is dependent upon film diffusion as the values lie between 10^{-6} to 10^{-8} for Zn^{2+}, Ni^{2+} and Cu^{2+} ions (Table 6.5).

The value of N_k was observed between 10^{-4} and 10^{-3}, which elucidated that adsorption was controlled by transfer controlled. Higher value of N_k results in enhanced adsorption of Ni^{2+} and Cu^{2+} ions. The value of φ and λ were in the range of 10^{-2} to 10^{4} and 10^{-12} to 10^{8}, which showed thorough coverage of composite surface during adsorption with trim downed surface tension [213], [272].

Table 6.5: Value of dimensionless numbers for ternary metal ions

Dimensionless numbers	φ	λ	N_k	D_P $\left(cm^2sec^{-1}\right)$	D_F $\left(cm^2sec^{-1}\right)$
Cu^{2+}	66.22	0.00013	0.00310	1.9×10^{-5}	2.00×10^{-7}
Ni^{2+}	66.89	3.29×10^{-5}	0.00307	1.9×10^{-5}	8.12×10^{-7}
Zn^{2+}	65.17	0.00028	0.00079	1.9×10^{-5}	9.04×10^{-7}

6.2.4 ANN Modeling

pH, AC dose, adsorbate concentration, contact time and temperature were provided as network inputs. The back-propagation technique with the L-M algorithm was used to predict output function. The network was trained until lesser number of epochs were obtained [235]. Thereafter, the network simulation was processed with the experimental data. The predictive output function was compared with the experimental results. Figure 6.7 shows the MSE of the ANN model obtained in training, testing and validation of data. The lowest MSE (encircled point) was recorded during training, testing and validation of data by L-M algorithm. Similar results were found by Yildiz, 2018 [232] with best

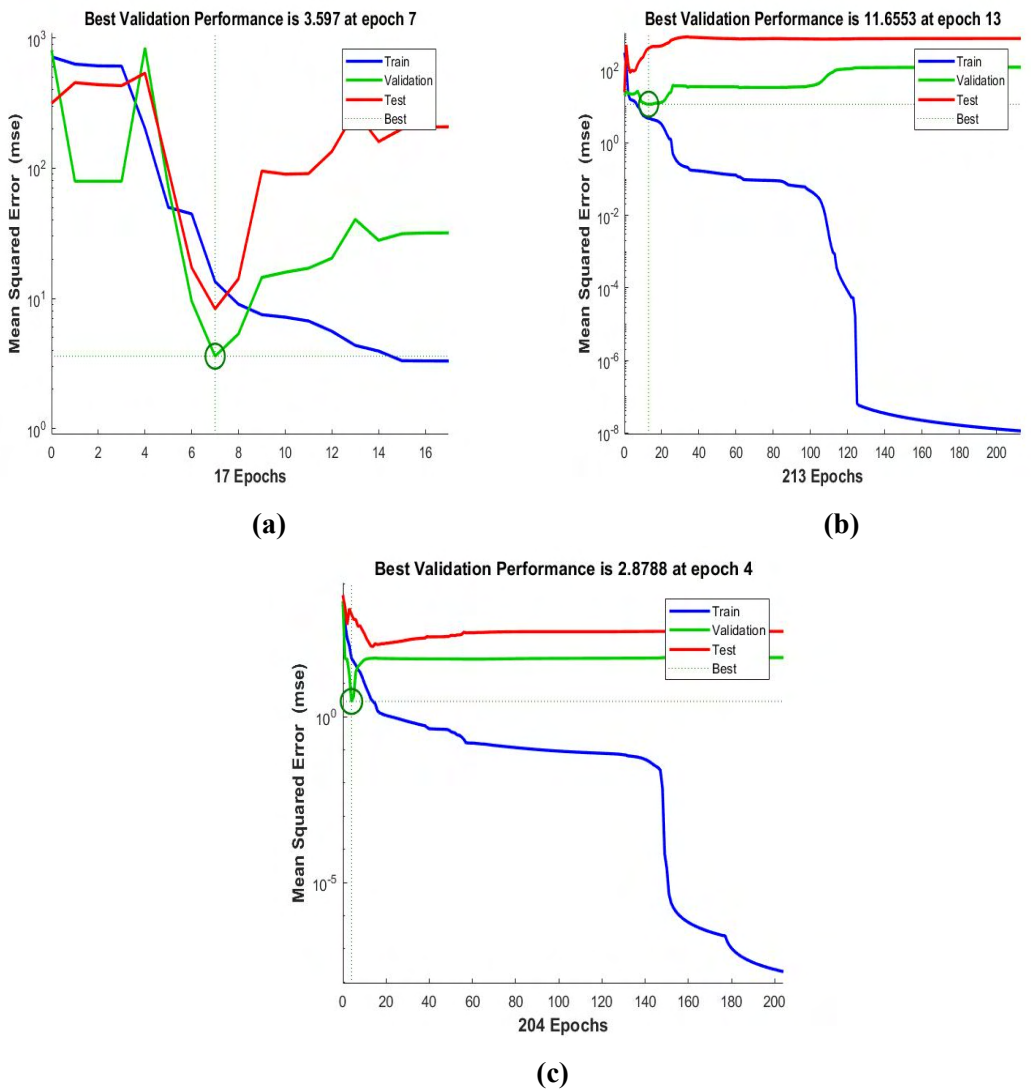

Figure 6.7: Performance between number of epochs and MSE for prediction of (a) Ni^{2+}, (b) Cu^{2+} and (c) Zn^{2+} ions removal using AC

validation performance 0.0011846 at epochs 27 for Ni^{2+} ions. Figure 6.8 shows regression between experimental and predicted values for the adsorption of Ni^{2+}, Cu^{2+} and Zn^{2+} ions on AC. The circles in the plot are experimental values and the colored lines show the predicted values derived from ANN models.

Both the experimental and theoretical values seemed to be in agreement with each other showing a high regression coefficient (R^2 value in range of 0.97 - 0.99) (Figure 6.8). Thus, in the present work, the L-M algorithm was concluded appropriate for predicting the output function with the lowest MSE at epoch (7, 13, 4 for Ni^{2+}, Cu^{2+} and Zn^{2+} ions) coupled and highest validation performance in ten neurons at 3.597, 11.6553 and 2.8788 for Ni^{2+}, Cu^{2+} and Zn^{2+} ions, respectively (Figure 6.7).

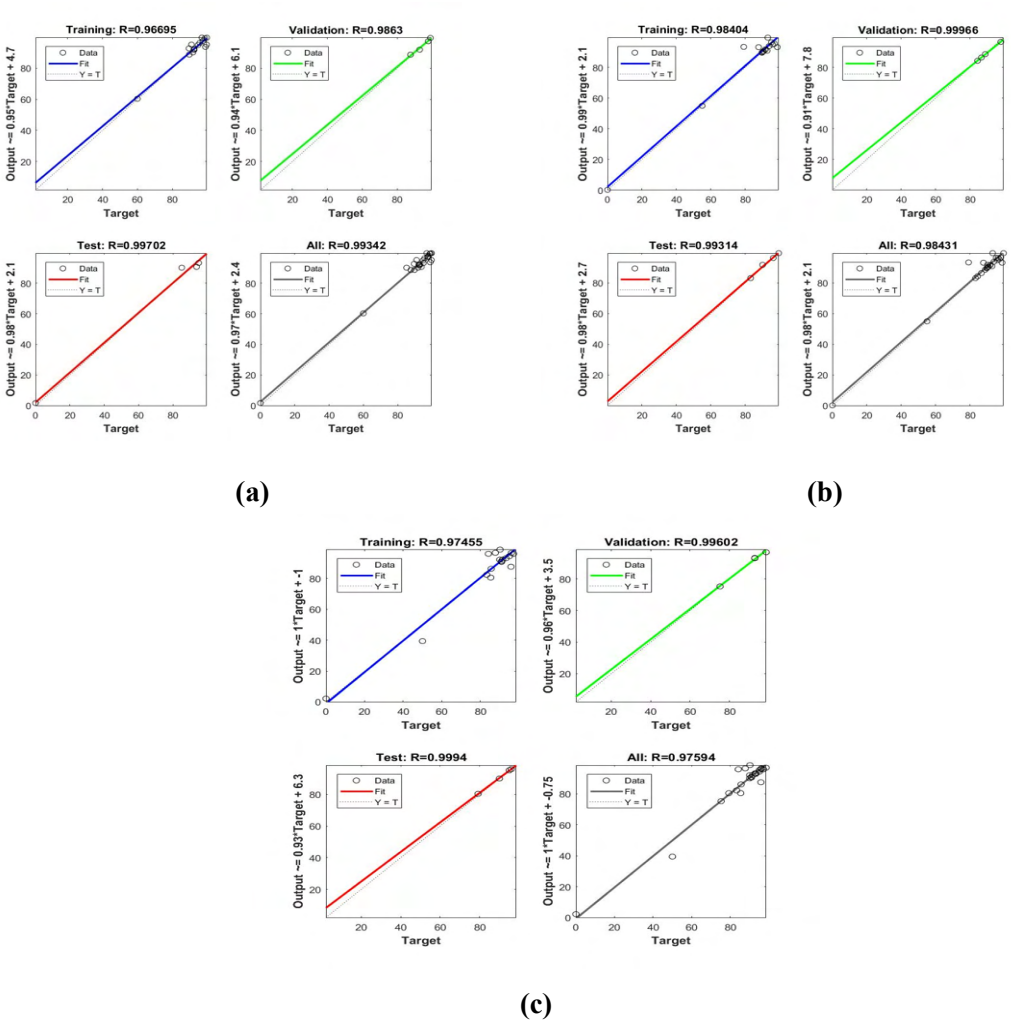

Figure 6.8: Regression plot for (a) Ni^{2+}, (b) Cu^{2+} and (c) Zn^{2+} ions

The results also showed a small deviation of 0.0081% for Ni^{2+}, 0.70% for Cu^{2+} and 0.30% for Zn^{2+} ions between the experimental and predicted values (Figure 6.9). This further showed the suitability of L-M algorithm in the present work. ANN were also used for modeling Cu^{2+} adsorption on zeolite surface [273].

Adsorbent dose, contact time and pH were given as input for simulating experimental results. Sobhani et al., 2018 [273] observed that the L-M back-propagation training function with ten neurons in the hidden layer were the most efficient network, similar to the present study.

Similarly, Yildiz, 2018 [232] applied ANN in the adsorption of Ni^{2+} from aqueous solution on peanut shell surface and found a high regression coefficient ((R) training (0.99), test (0.97) and validation (0.99)) between experimental and predicted values.

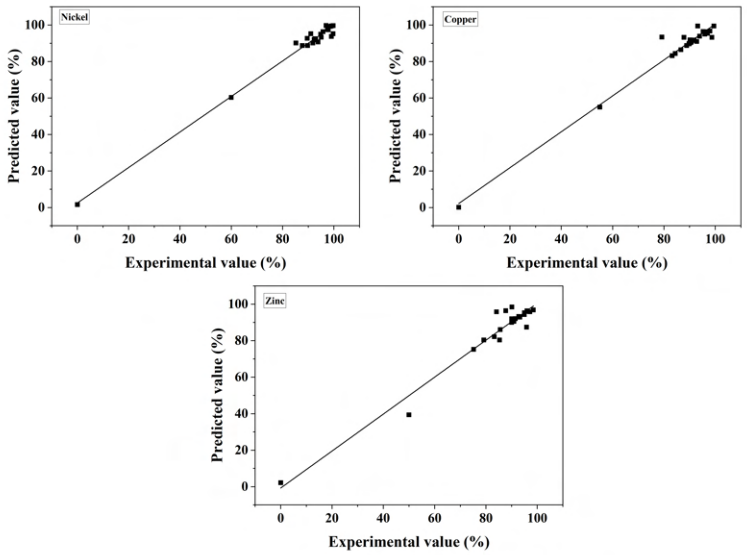

Figure 6.9: Correlation plot for the experimental and ANN predicted values

6.2.5 Adsorption Kinetics

It is evident from Figure 6.10 that adsorption of Cu^{2+}, Ni^{2+} and Zn^{2+} ions did not fit the PFO model.

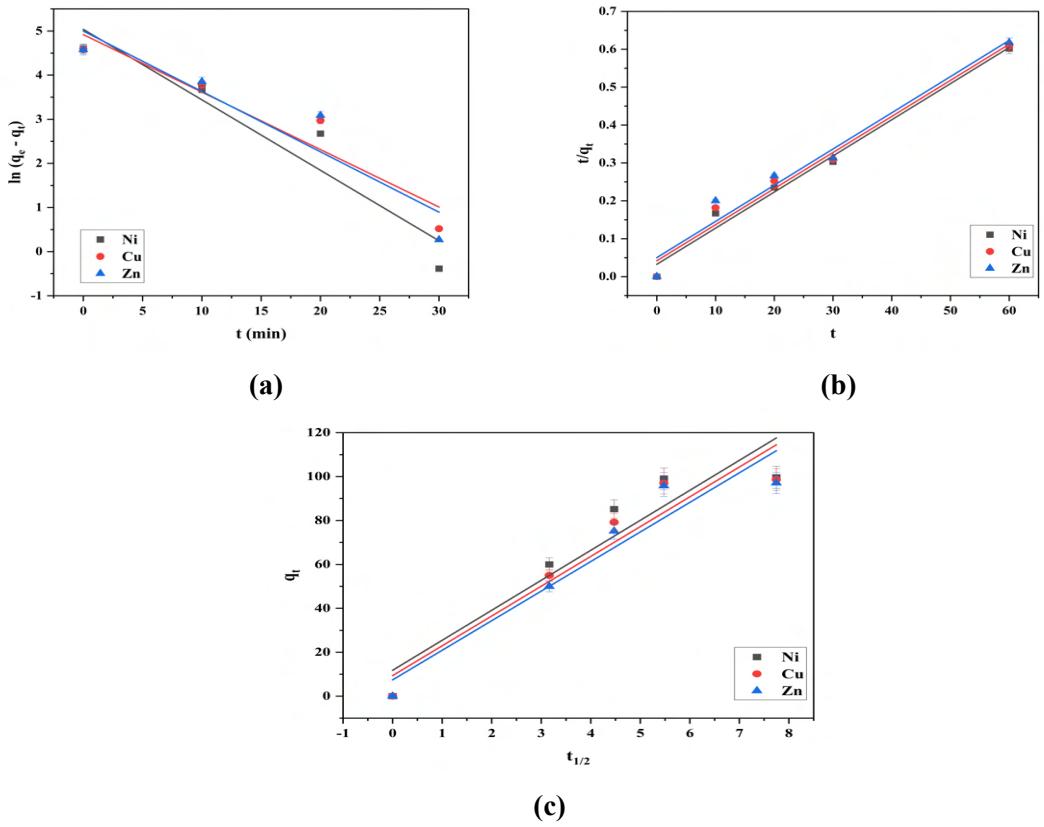

(a) **(b)**

(c)

Figure 6.10: (a) PFO, (b) PSO and (c) IPD model for AC as adsorbent

The PSO kinetic model shown in Figure 6.10 demonstrated a higher linearity agreement.The higher correlation coefficients (Table 6.6) and predicted q_e values of PSO model indicated that, it was suitable to describe the adsorption kinetic of Cu^{2+}, Ni^{2+} and Zn^{2+} ions onto AC, which is consistent with the results reported in Bouhamed et al., 2012 [415]. Consequently, it can be concluded that the mechanism of adsorption of metal ions included chemical adsorption. This kinetic model appears to be realistic due to the observed chemical modifications as confirmed by the FTIR results. Sabela et al., 2019 [416] performed removal of Cu^{2+} by using activated carbon derived from green vegetables waste and found PSO kinetics better fitted in the experimental data. Their findings are similar to the present study.

Table 6.6: Adsorption kinetic model parameters for AC as adsorbent

Kinetic Parameter		PFO		PSO		IPD	
		q_e (mg/g)	k_1 min^{-1}	q_e (mg/g)	k_2 (g/mg. min)	k_p (mg/g. min)	C (mg/g)
Value	Cu^{2+}	137	0.13	105.04	0.002	13.56	9.36
	Ni^{2+}	154.47	0.16	104.82	0.003	13.66	11.79
	ZN^{2+}	146.94	0.14	104.60	0.001	13.46	7.43
R^2	Cu^{2+}	0.91		0.98		0.91	
	Ni^{2+}	0.91		0.98		0.89	
	Zn^{2+}	0.88		0.97		0.92	

6.2.6 Adsorption Isotherm

The adsorption of ternary metal ions on the AC followed the Freundlich isotherm model very well with the higher values of R^2 (0.97-0.98) (Table 6.7), and also fit in to the Langmuir isotherm model with the values of R^2 (0.96), but not better than the Freundlich isotherm model in general (Figure 6.11).

In D-R isotherm, the value of 'E' was < 8 kJ/mol establishing the role of physical adsorption on the surface of AC [278]. In Freundlich isotherm, 'n' was > 1 which indicated

towards favorable adsorption [279]. Freundlich isotherm were also better fitted in a study done by Mohan and Singh, 2002 [290] during adsorption of cadmium and zinc using activated carbon.

Multi-metal systems function in the same way with nickel as the most efficient adsorbate and zinc as the least. Ni^{2+} ions (0.069 nm) have the lowest ionic radius of all ions, implying faster adsorption. The second most adsorbed metal is Cu^{2+} ions (0.073 nm), followed by Zn^{2+} ions (0.074 nm). This indicates that the adsorption of Cu^{2+}, Ni^{2+} and Zn^{2+} ions on AC followed the opposite trend of ionic radius, i.e., $Ni^{2+} > Cu^{2+} > Zn^{2+}$. The adsorption capacity of the metal ions has been shown in Table 6.7.

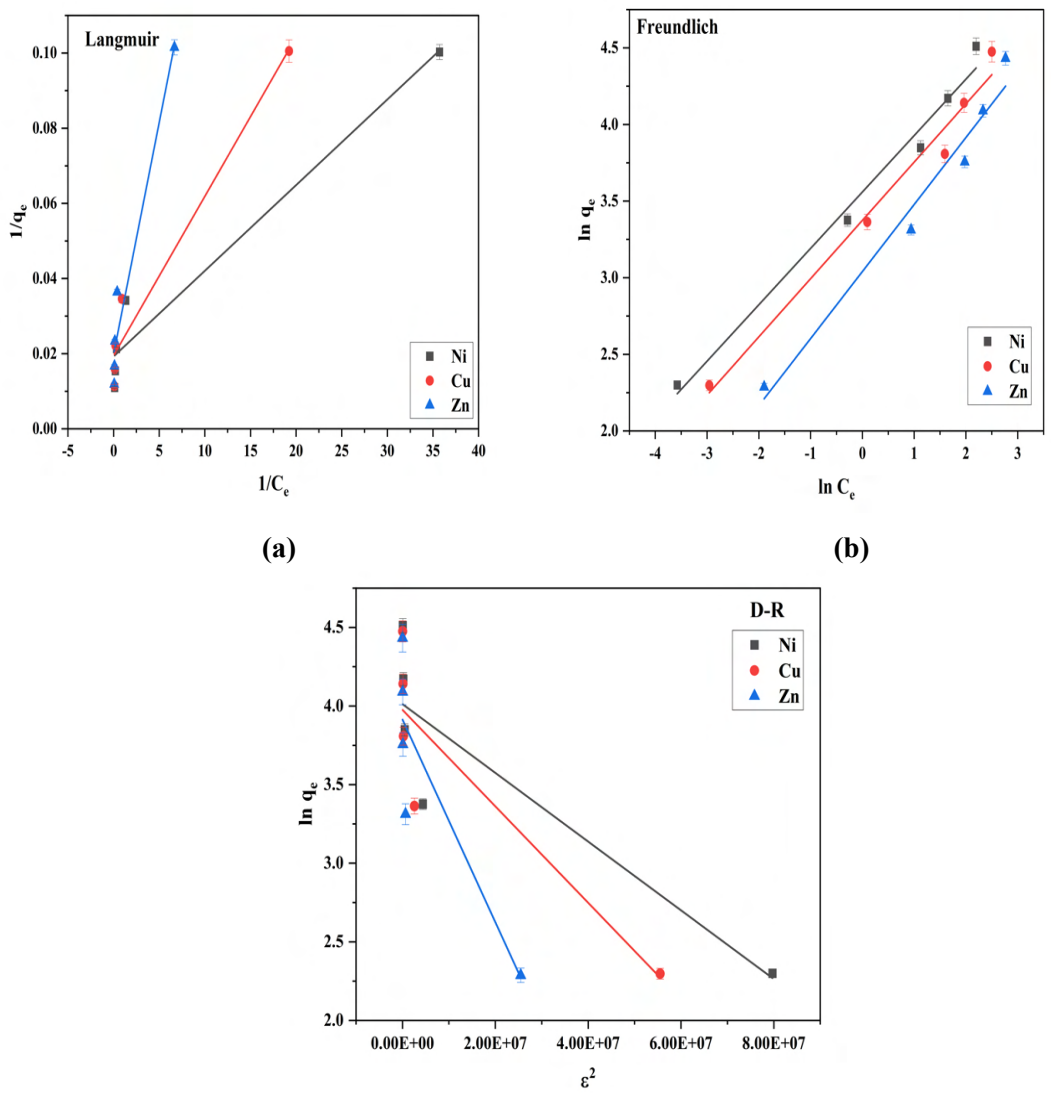

Figure 6.11: (a) Langmuir, (b) Freundlich and (c) D-R model for AC as adsorbent

Table 6.7: Adsorption isotherm model parameters for AC as adsorbent

Isotherm		Langmuir		Freundlich		D-R	
Parameter		q_m (mg/g)	K_L (L/mg)	n	K_F (L/mg)	E (J/mol)	q_m (mg/g)
Value	Cu^{2+}	250	0.21	2.63	29.08	916.69	52.98
	Ni^{2+}	500	0.10	2.70	35.16	531.49	55.15
	Zn^{2+}	83.33	0.60	2.32	20.90	1507.55	0.003
R^2	Cu^{2+}	0.96		0.98		0.79	
	Ni^{2+}	0.96		0.98		0.79	
	Zn^{2+}	0.96		0.97		0.77	

6.2.7 Thermodynamics

The value of ΔG was negative and decreased with the rise in temperature from 288 to 308 K which pointed towards the feasible and spontaneous adsorption of Cu^{2+}, Ni^{2+} and Zn^{2+} ions at higher temperature (Figure 6.12) [274]. Furthermore, the value of ΔG was <

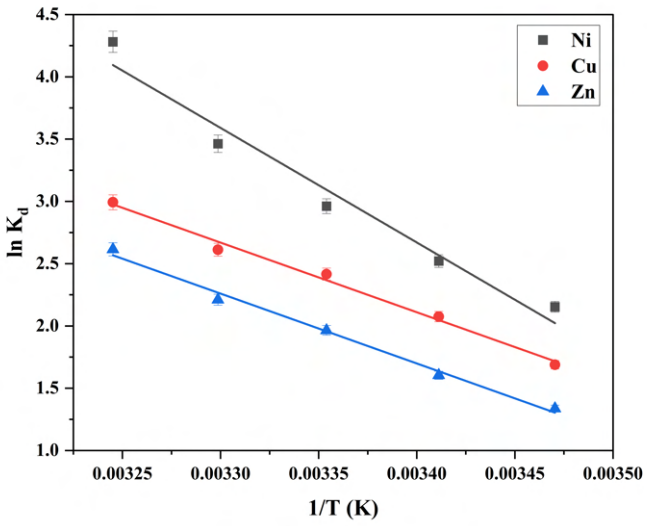

Figure 6.12: Plot of ln K_d vs 1/T for AC

20 kJ/mol (Table 6.8) which showed the possibilities of electrostatic interaction between active sites of AC and ternary metal ions [283]. The positive value of ΔH suggested the endothermic adsorption [284]. The positive ΔH can be explained by the fact that the metal ion hydration sphere is destroyed before the ternary metal ions adsorption took

place on the AC. The dehydration consumed energy and is preferred at higher temperatures [284], [285]. The positive value of ΔS depicted increased randomness at the solid-aqueous interface [232], [286]. When Bouhamed et al., 2016 [319] tested the adsorption of copper, nickel, and zinc from aqueous solutions onto activated carbon made from date stones, they got comparable findings.

Table 6.8: Thermodynamic parameters for ternary metal ions adsorption

Temperature (K)		288	293	298	303	308
ΔG (J/mol)	Cu	-4110.09	-4988.05	-5866.01	-6743.97	-7621.93
	Ni	-4841.49	-6252.38	-7663.27	-9074.16	-10485
	Zn	-3126.03	-3989.44	-4852.84	-5716.25	-6579.66
ΔGS (J/mol K)	Cu	175.59				
	Ni	282.17				
	Zn	172.68				
ΔGH (J/mol)	Cu	46486.65				
	Ni	76467.85				
	Zn	46632.23				

6.2.8 Optimization Study

6.2.8.1 Effect of pH

With the rise in pH, the percentage adsorption of ternary metal ions increased (Figure 6.13). When the pH is between 8.8 to 10, copper is adsorbed as Cu^{2+}, $Cu(OH)^{+}$, and $Cu(Cl)^{+}$, nickel is adsorbed as Ni^{2+}, $Ni(OH)^{+}$, and $Ni(OH)^{3-}$ and zinc is adsorbed as Zn^{2+} and $Zn(OH)^{+}$ [288]. As pH_{zpc} is 8.56, the range of pH for obtaining the optimum pH was kept between 8.8 to 10. This is because at pH > pH_{zpc}, the surface is negatively charged and allow positively charged metal ions to adsorb on the surface. The pH is limited to 10 due to the fact that alternative forms of these metal ions are adsorbed on the surface in place of the Cu^{2+}, Ni^{2+} and Zn^{2+} ions [289], [290]. Bouhamed et al., 2015 [319] used the activated carbon made from date stones to perform multi-component adsorption of copper, nickel, and zinc from aqueous solutions. Bouhamed et al., 2015 [319] found that

the adsorbent has a pH_{zpc} of 3.34 and surface charge is negative above this, which helped in the adsorption of copper, nickel, and zinc ions. In their research, Bouhamed et al., 2015 [319] determined optimum pH for metal ion adsorption was pH 5.5. Yu et al., 2018 [417] prepared silver ferrocyanide-impregnated activated carbon and found pH_{zpc} of 7.25. Similar to the present study, pH_{zpc} of silver ferrocyanide-impregnated activated carbon was on the basic side of the pH scale.

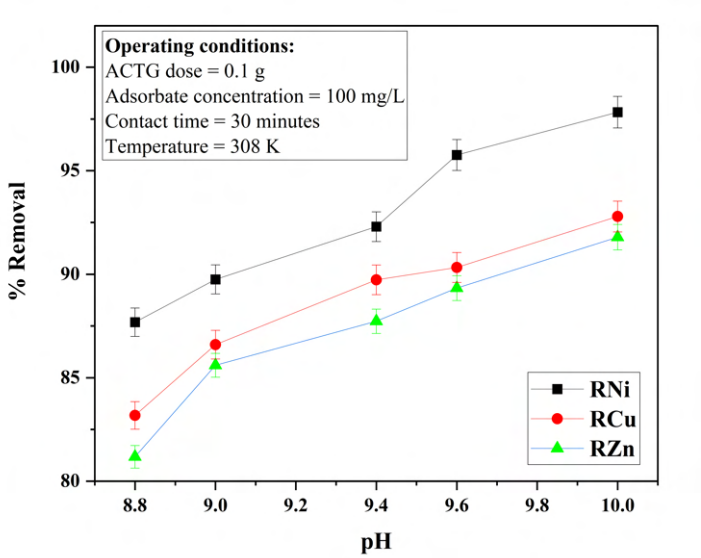

Figure 6.13: Effect of pH on percentage removal of ternary metal ions using AC

6.2.8.2 Effect of AC Dose

Figure 6.14 shows effect of AC dose on the percentage removal of Cu^{2+}, Ni^{2+} and Zn^{2+} ions and AC adsorption capacity. An increase in AC dose from 0.1 to 1 g resulted in enhanced percentage removal of Cu^{2+}, Ni^{2+} and Zn^{2+} ions. The amount of metal ions adsorbed increases from 91.8% to 99.10% for Ni^{2+}, 90.70% to 97.90% for Cu^{2+} and 90% to 96% for Zn^{2+}. The boosted percentage removal of Cu^{2+}, Ni^{2+} and Zn^{2+} was due to increased surface area and number of active sites available on the AC. However, adsorption capacity demonstrated an opposite pattern to percentage removal. Adsorption capacity of composite decreased from 91.80 to 9.91 mg/g for Ni^{2+}, 90.70 to 9.79 mg/g for Cu^{2+} and 90 to 9.6 mg/g for Zn^{2+}, respectively. This decrease was attributed to the overlapping or grouping of active sites which increases the diffusion path length for metal ions to the AC surface. Alatabe, 2018 [418] determined that a 3 g adsorbent dose was optimum for the ad-

sorption of Cu^{2+} ions from aqueous solution onto activated carbon synthesized from cane papyrus. Similarly, Copper, nickel, and lead ions from synthetic semiconductor industry effluent were adsorbed by palm shell activated carbon by Onundi et al., 2010 [419], who discovered that 1 g was the optimal amount of adsorbent to use because the adsorption capacity decreased after this amount.

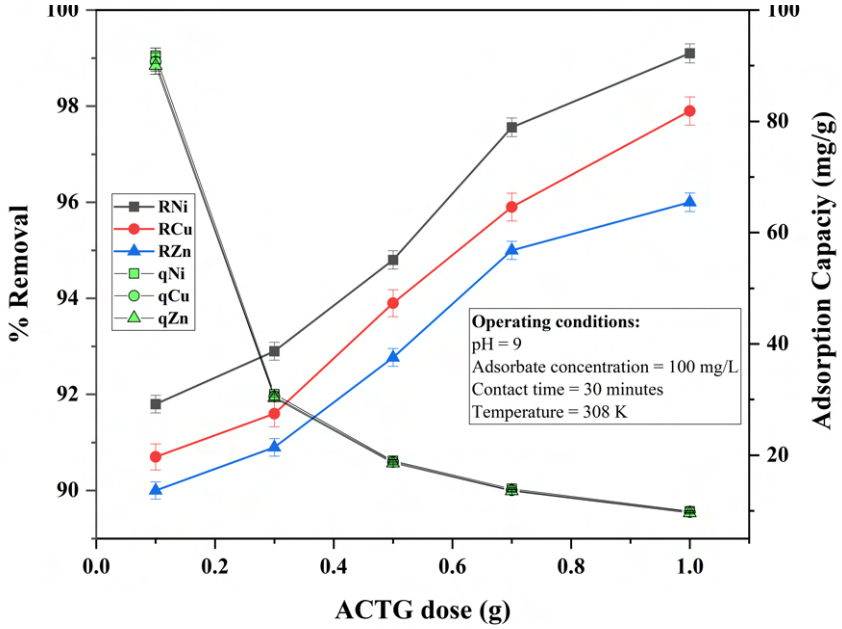

Figure 6.14: Effect of AC dose on percentage removal of ternary metal ions and adsorption capacity of AC

6.2.8.3 Effect of Initial Concentration

It is evident from Figure 6.15 that percentage removal decreased from 99.72% to 91%, 99.48% to 87.8% and 98.5% to 84.11% for Cu^{2+}, Ni^{2+} and Zn^{2+} ions, respectively as the metal's concentration increased from 10 to 100 mg/L. Such a reduction was attributed to a fixed number of active sites in the AC, and all active sites were completely occupied at higher metal concentrations. The adsorption capacity of AC augmented with an increase in the metal ion concentration. This increase was attributed to increased concentration gradient, a driving force for overcoming the mass transfer resistance between metal ions and the solid phase. Similar to the present study, Alatabe, 2018 [418] determined that copper ion concentration of 3 ppm was optimum for the adsorption of Cu^{2+} ions from aqueous solution onto activated carbon synthesized from cane papyrus.

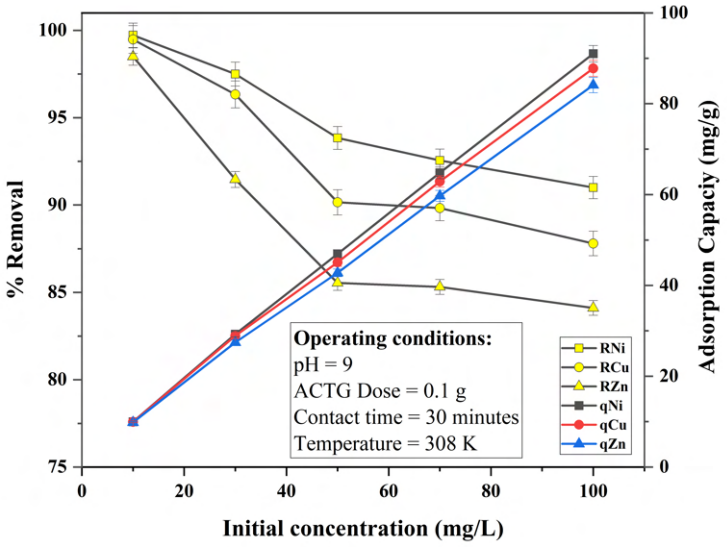

Figure 6.15: Effect of initial concentration of Ni^{2+}, Cu^{2+} and Zn^{2+} ions on percentage removal and adsorption capacity of AC

6.2.8.4 Effect of Contact Time

The adsorption of ternary metal ions on AC increased with escalation of contact time up to 30 minutes (Figure 6.16). Thereafter, there were no significant increase in the removal

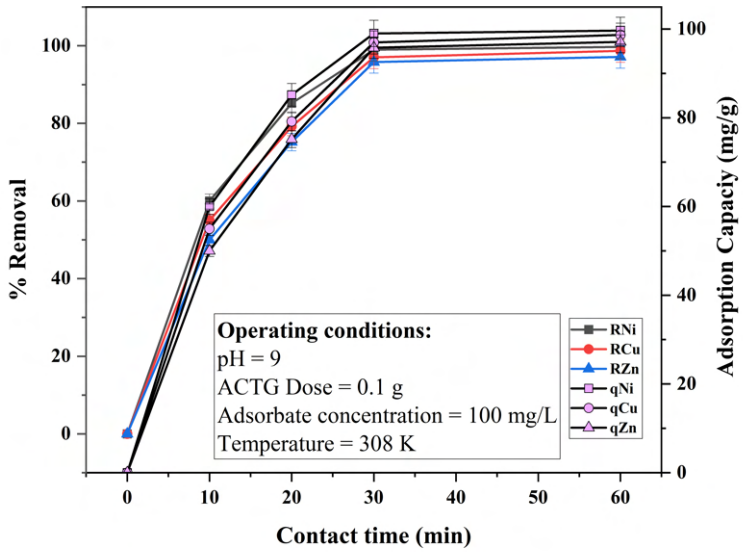

Figure 6.16: Effect of contact time on percentage removal of ternary metal ions and adsorption capacity of AC

of these metal ions. Significant removal of ternary metal ions occurred in mentioned time and the order of adsorption of metal ions was $Ni^{2+} > Cu^{2+} > Zn^{2+}$. The order is in opposite to ionic radius of metal ions that follows the order as: $Ni^{2+} < Cu^{2+} < Zn^{2+}$. The metal ion

with smallest ionic radius was the first to adsorb. Similar results were found by Abdulrazak et al., 2017 [420] during removal of copper, nickel and cadmium using activated carbon prepared from African palm fruit. Likewise, Alatabe, 2018 [418] determined that contact time of 120 minutes was optimum for the adsorption of Cu^{2+} ions from aqueous solution onto activated carbon synthesized from cane papyrus. Similar to the present work, Onundi et al., 2010 [419] used palm shell activated carbon to adsorb copper, nickel, and lead ions from synthetic semiconductor industry effluent and reported that the equilibrium contact time for lead ions was 60 minutes and 75 minutes for copper and nickel ions.

6.2.8.5 Effect of Temperature

The effect of temperature on adsorption of ternary metal ions is shown in Figure 6.17.

It is evident from Figure 6.17 that the adsorption of metal ions improved with an increase

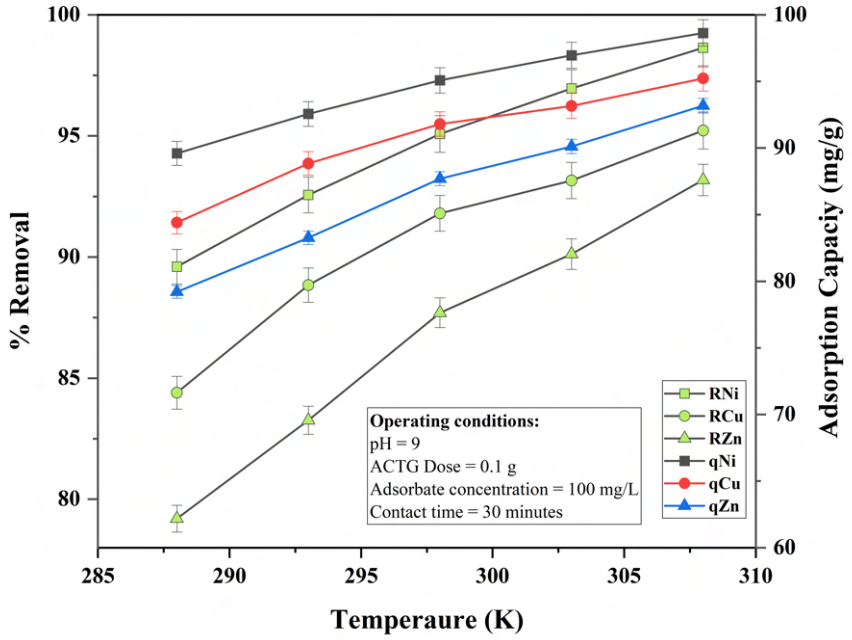

Figure 6.17: Effect of temperature on percentage removal and adsorption capacity of AC

in temperature from 288 to 308 K. This showed that the adsorption of Cu^{2+}, Ni^{2+} and Zn^{2+} was endothermic. Increased adsorption at higher temperature was attributed to generation of more active surface sites on the composite and reduced boundary thickness around the composite which reduced the mass transfer resistance in the boundary layer [297]. Thus, 35°C is regarded as the optimum temperature for further studies. A study by

Onundi et al., 2010 [419] used palm shell activated carbon at 27°C to bind nickel, copper and lead ions from synthetic semiconductor industrial effluent. At a temperature of 298 K, Aboli et al., 2020 [421] studied the adsorption of cobalt, lead and nickel ions from aqueous solution onto activated carbon made from mousambi leaves.

6.3 Adsorption mechanism for AC

The adsorption mechanism between sawdust and heavy metal ions is a significant topic for discussion [422]. In the past few years, scientists have been studying how sawdust adsorbs heavy metals. They found that ion exchange and hydrogen bonding were the most important mechanisms [423].

These concepts were supplemented by the TG's constituents and complexing capabilities, heavy metal characteristics and adsorption behaviour such as the impact of pH on aqueous solutions. There are a number of complexes which can be formed between ternary metal system and O-, S-, or K- containing groups in AC [423]. Compounds that are capable of participating in an ion exchange include cellulose, lignin, carboxylic acids, aldehydes, and numerous hydroxyl groups. The polymer lignin found in AC is a component of the TG.

Extraction sites like Na, S and Cl being incorporated in AC was due to the TG modification process. The ion exchange process may be preferred because of the electron-donating character of AC's O- and S-containing groups and the electron-accepting nature of ternary metal ions. Cu^{2+}, Ni^{2+} and Zn^{2+} are all divalent heavy metal ions that binds with two adjacent hydroxyl and phenolic groups, donating two pairs of electrons to the ternary metal ions. This reaction produces four coordination number compounds and releases two hydrogen ions into solution. The following equations demonstrate these mechanisms by Eqs. 6.1, 6.2 and 6.3 [423].

- **Ion exchange**

$$2\,(-ROH) + M^{2+} \rightarrow 2\,(RO)\,M + 2H^{+} \tag{6.1}$$

$$-ROH + M(OH)^{+} \rightarrow (-RO)M(OH) + H^{+} \tag{6.2}$$

- **Hydrogen bonding**

$$2(-ROH) + M(OH)_2 \rightarrow (ROH)_2 + M(OH)_2 \tag{6.3}$$

where, R represents AC and M to ternary metal ions.

The surface complexes and functional groups also had an impact on the AC's adsorption ability. FTIR analysis of AC was used to determine the active functional groups involved in chemical reactions (Figure 6.3). Before and after the ternary metal ions adsorption, there were displacements in the AC. Firstly, the intensity of almost all of the infrared bands appeared to decline, and the decreasing vibration intensity indicated that such material had undergone chemical changes [11]. There were evident displacements at 3422.27 to 3409.84 cm^{-1}, 1633.63 to 1618.87 cm^{-1} and 669.29 to 614.22 cm^{-1} showed adsorption involves OH, C=O stretching and C=C bending. Whewellite ($CaC_2O_4.H_2O$), a hydrated calcium oxalate mineral, was also found in AC. Calcium ions are electrovalently linked to carboxylate ions, making it easier for metal ions to get exchanged with calcium ions. Thus, ion exchange, hydrogen bonding and complexation are the main mechanism responsible for adsorption of M^{2+} on composite.

6.4 Comparative Study

Table 6.9 shows a comparison of the physicochemical parameters of activated carbon produced from wood waste using distinct activating agents. The following table compares the physical and chemical parameters of activated carbon obtained from different types of wood waste to the precursor used to prepare activated carbon in this study. The findings in Table 6.9 reflect a statistically significant comparison of the specific area, yield (%), iodine number, bulk density, pH_{zpc}, fixed carbon, volatile carbon, ash, and moisture content of activated carbon generated from various types of wood waste and the one employed in this study.

Table 6.9: Comparative analysis of the physico-chemical features of AC with those of other activated carbons

Wood waste	***Tectona grandis***	**Poplar sawdust**	**Pods of golden shower (GS)**	**Sago Palm Bark**	**Teak s awdust**	**Teak sawdust**	**Teak (Tectona Grandis) wood**	**Sawdust**
Activation reagent	Zinc chloride	Zinc chloride	Potassium carbonate	Zinc chloride	Steam	chicken dropping compost ash (CCA) and empty fruit bunch ash (EFBA)	Zinc chloride	Steam
BET Surface area (m/g)	585	1100	-	1737	1150	930	996.7	516.3
Yield (%)	42	-	57.67	-	-	-	-	-
Bulk Density (g/cm)	0.96	-	0.11	-	-	-	-	0.38
Iodine number (mg/g)	1036	-		-	-	-	-	-
Fixed carbon (%)	-	13.1	20.93	-	28.09	22.4	-	-
Volatile matter (%)	-	75	76.23	-	63.3	76.77	-	-
Ash (%)	9.4	4	1.17	1.5	0.4	0.8	-	6.5
Moisture (%)	11.35	7.9	1.8	9	7.4	7.48	-	0.52
pH_{zpc}	-	-	8.15	-	-	-	-	-
Reference	[424]	[425]	[426]	[427]	[407]	[183]	[330]	[428]

Wood waste	**Rubber wood sawdust**	**Sawdust**	**Gamhar (White teak) sawdust**	**Pine sawdust**	**Acacia arabica sawdust**	**Casuarina**	**Rubberwood sawdust**	**Raw sawdust**	***Tectona grandis sawdust***
Activation reagent	Phosphoric acid	Phosphoric acid	Phosphoric acid	Phosphoric acid	Zinc chloride	Phosphoric acid	Steam activation	Potassium hydroxide	Sodium thiosulphate
BET Surface area (m2/g)	1496	1536	310.23	1000	905	-	1092	784	1270
Yield (%)	35	43.8	-	-	-	69.2	-	58	72.8
Bulk Density (g/cm3)	-	-	-	-	-	0.42	-	-	0.42
Iodine number (mg/g)	1096	-	-	-	670	1186	765	-	782
Fixed carbon (%)	23.38	-	15.8	14.7	81	67.7	24.15	21.9	36.91
Volatile matter (%)	69.68	-	72.77	75.3	15	5.7	62.91	77.5	55.4
Ash (%)	0.74	-	0.73	0.6	1	10.3	4.95	0.6	7.3
Moisture (%)	6.2	-	10.7	9.4	3	16.3	-	17.3	0.39
pH_{zpc}	-	-	-	-	-	6.8	-		8.56
Reference	[412]	[429]	[329]	[430]	[431]	[432]	[433]	[434]	Present study [435]

The BET surface area obtained in this study is equivalent to that of other activated carbons earlier reported in Table 6.9. Additionally, a comparison of AC with other adsorbents in relation to pH, initial adsorbate concentration, best isotherm and kinetics fitted with maximum adsorption capacity has been done and shown in Table 6.10. It became apparent that AC is one of the best novel adsorbent for adsorption of heavy metal ions from the aqueous phase due to higher adsorption capacity.

Table 6.10: Comparison of various adsorbents with AC

Nickel						
Adsorbent	**pH**	**Initial concentration (mg/L)**	**Best fitted isotherm model**	**Best fitted kinetic model**	**Adsorption capacity (mg/g)**	**Ref**
Tea waste	-	100	-	-	5.72	[436]
Bagasse fly ash	6	100	Freundlich	-	6.48	[377]
Starch	7.5	100	-	PSO	96	[437]
Wood charcoal	7.5	100	-	PSO	99	[437]
Activated charcoal	7.5	100	-	PSO	99.6	[437]
Clay	7.5	100	-	PSO	99.6	[437]
Clinoptilolite	7	25	Langmuir	PSO	1.6	[438]
pomegranate peel waste	5.5 - 6.5	-	Langmuir	PSO	52	[439]
Kenaf	4.5	100	Langmuir	-	41.66	[440]
Cashew nut shell	5	50	Langmuir	PSO	18.86	[346]
Nettle Ash	6	100	Langmuir	PSO	192.3	[441]
Pine sawdust	3.9	2.625	Freundlich	-	65.9×10^{-3}	[442]

Groundnut shell	6.32-6.41	-	-	PSO	0.36	[443]
Watermelon rind	5	50	-	-	35.3	[444]
Grapefruit peel	5	50	Freundlich	PSO	46.13	[445]
Hemp Fibers	5	100	Langmuir-Freundlich	PSO	242	[446]
Coconut coir pith	6	50	Langmuir	PSO	24.39	[447]
Peat	5	50	Langmuir	PSO	61.27	[125]
Pistachio Hull waste	04-Jun	100	Freundlich	PSO	14.1	[448]
A. barbadensis Miller leaves (ABL)	7	100	Freundlich	PSO	10	[449]
AC	**9**	**100**	**Freundlich**	**PSO**	**500**	**Present study**
			Copper			
Adsorbent	**pH**	**Initial concentration (mg/L)**	**Best fitted isotherm model**	**Best fitted kinetic model**	**Adsorption capacity (mg/g)**	**Ref.**
Bentonite	7	100	Langmuir	-	5.4	[450]
Lentil shells	6	100	Langmuir	PSO	9.59	[370]
Wheat shells	6	100	Freundlich	PSO	17.42	[370]
Rice shells	6	100	Langmuir	PSO	2.95	[370]
Newspaper Pulp	7	20	Langmuir	PSO	30	[451]

Unye clay	6	6.4	Freundlich	-	105.38	[452]
Hazelnut husk Activated carbon	5.7	200	Langmuir	-	6.645	[453]
Cinnamomum camphora	4	100	Langmuir	PSO	17.87	[454]
Pomegranate peel	5.8	-	Langmuir	PSO	-	[455]
Watermelon shell	8	20	Langmuir	PSO	111.1	[456]
Brazilian bentonite clay	-	-	-	-	5.23	[311]
Clay soil	5.7	100	Dubinin Radushkevich	PSO	28.57	[457]
Bentonite	6	100	Langmuir	PFO	248.9	[206]
Bentonite and Graphene oxide composite	6	100	Langmuir	PFO	558.4	[206]
Modified Nano-bentonite	7.3	110.1	Langmuir	-	19.92	[458]
Saudi Clay	6	500	Langmuir	PSO	32.36	[294]
AC	**9**	**100**	**Freundlich**	**PSO**	**250**	**Present study**
			Zinc			
Adsorbent	**pH**	**Initial concentration (mg/L)**	**Best fitted isotherm model**	**Best fitted kinetic model**	**Adsorption capacity (mg/g)**	**Ref.**

Fish Scales	3	60	Langmuir-Freundlich	Generalized Elovich	15.38	[459]
Orange Peel	-	40	-	-	37.64	[460]
Pomegranate Peel	-	40	-	-	37.17	[460]
Pineapple Peel	-	40	-	-	36.99	[460]
Groundnut Husk Ash	-	40	Langmuir	PSO	56.5	[52]
Bentonite clay	5.5	10250	-	-	437.16	[461]
Kaolinite clay	6	100	Freundlich	PSO	6.35	[462]
Bentonite clay	6	100	Langmuir	PSO	79.2	[462]
Natural clay	6	150	Langmuir	PSO	5.7	[463]
Cationic Surfactant Modified Bentonite	6	200	Langmuir	PSO	35.21	[464]
Ethylenediam-inetetraacetic Acid-Modified Bentonite	4	-	Langmuir	PSO	2.77	[465]
Kaolin	5.84	2.15	Jovanovic and Redlich-Peterson	Avrami	60.39	[466]

Natural Allophane	8.5	100	Langmuir	Pseudo-First-Order	20.9	[467]
Synthetic Allophane	8.5	100	Langmuir	Pseudo-First-Order	26.9	[467]
Synthetic Allophane	8.5	100	Langmuir	Pseudo-First-Order	36.9	[467]
Clay soil	5.7	100	Dubinin Radushkevich	PSO	24.39	[457]
Modified Nano-bentonite	6.9	105	Langmuir	-	18.52	[458]
AC	**9**	**100**	**Freundlich**	**PSO**	**83.33**	**Present study**

6.5 Biodegradability Study

Activated carbon is formed when formerly substances are burned, dehydrated, and evaporated. Due to the fact that activated carbon is derived from coal, it has been classified as an organic substance. It has been found that aromatic compounds such as phenols are difficult to break down when drinking water is treated with activated carbon, as per the National Research Council (US) [468]. As per the FTIR analysis (Figure 6.3), AC is constituted of specific organic compounds that cannot be decomposed. As a result, AC were classified as non-biodegradable.

6.6 Conclusion

The present study developed a simple, quick, and environmentally friendly carbonization approach for synthesizing activated carbon from *Tectona grandis* (sago waste). Proximate analysis determined the moisture, ash, and fixed carbon contents in TG to be 18.3 %, 0.7

%, and 67.7 %, respectively. The high fixed carbon content of TG suggested that the sawdust contained 67.7 % non-volatile carbon. This proximate analysis provides insight into the carbon quality generated from precursor material. The SEM picture revealed that the porosity of AC was caused by TG being chemically activated. FTIR spectra were used to verify the presence of oxygenated functional groups on the surface of TG, including lactone, phenols, carboxylic acids, aldehydes, and aryl halide. The present work determined an iodine concentration of 782 mg/g (SD ± 0.27), indicating the presence of micropores on the surface of AC. The XRD pattern revealed that AC is amorphous. The enormous BET surface area (1270 m^2/g) and total pore volume (0.673 cm^3/g) suggested that AC had a large specific surface area available for adsorption. Cu^{2+}, Ni^{2+} and Zn^2 ions adsorption onto AC is found to be pH, initial concentration, temperature, contact time, and AC dose dependent. The adsorption procedure demonstrated a brisk initial uptake and equilibrium was reached in around 60 minutes. The pH value of 9 was found to be optimal, initial concentration of 100 mg/L, contact time of 30 minutes, temperature of 308 K, and AC dose of 0.10 g. The experimental results suggested that the PSO kinetics model fit the data the best. The isotherm analysis found that the Freundlich isotherm model best fits the experimental isotherm data. This method produces non-biodegradable activated carbon. Thus, when applied as an adsorbent, AC helps in the treatment of industrial wastewater.